Journal for ImmunoTherapy of Cancer

TGM4: an immunogenic prostate-restricted antigen

Zoila A Lopez-Bujanda ,[1,2,3,4] Aleksandar Obradovic ,[2] Thomas R Nirschl ,[1,3] Laura Crowley,[5,6,7,8,9] Rodney Macedo ,[2] Alexandros Papachristodoulou ,[6,10] Timothy O'Donnell,[11] Uri Laserson ,[11] Jelani C Zarif,[3,12] Ran Reshef ,[2,13] Tiezheng Yuan,[14,15] Mithil K Soni,[2] Emmanuel S Antonarakis ,[12] Michael C Haffner ,[16] H Benjamin Larman,[14,15] Michael M Shen ,[5,6,7,8,9] Pawel Muranski ,[2,7] Charles G Drake [2,9,13]

To cite: Lopez-Bujanda ZA, Obradovic A, Nirschl TR, *et al*. TGM4: an immunogenic prostate-restricted antigen. *Journal for ImmunoTherapy of Cancer* 2021;**9**:e001649. doi:10.1136/jitc-2020-001649

► Additional material is published online only. To view, please visit the journal online (http://dx.doi.org/10.1136/jitc-2020-001649).

Accepted 08 March 2021

Check for updates

© Author(s) (or their employer(s)) 2021. Re-use permitted under CC BY-NC. No commercial re-use. See rights and permissions. Published by BMJ.

For numbered affiliations see end of article.

Correspondence to
Dr. Charles G Drake;
cgd2139@cumc.columbia.edu

ABSTRACT

Background Prostate cancer is the second leading cause of cancer-related death in men in the USA; death occurs when patients progress to metastatic castration-resistant prostate cancer (CRPC). Although immunotherapy with the Food and Drug Administration-approved vaccine sipuleucel-T, which targets prostatic acid phosphatase (PAP), extends survival for 2–4 months, the identification of new immunogenic tumor-associated antigens (TAAs) continues to be an unmet need.

Methods We evaluated the differential expression profile of castration-resistant prostate epithelial cells that give rise to CRPC from mice following an androgen deprivation/repletion cycle. The expression levels of a set of androgen-responsive genes were further evaluated in prostate, brain, colon, liver, lung, skin, kidney, and salivary gland from murine and human databases. The expression of a novel prostate-restricted TAA was then validated by immunostaining of mouse tissues and analyzed in primary tumors across all human cancer types in The Cancer Genome Atlas. Finally, the immunogenicity of this TAA was evaluated in vitro and in vivo using autologous coculture assays with cells from healthy donors as well as by measuring antigen-specific antibodies in sera from patients with prostate cancer (PCa) from a neoadjuvant clinical trial.

Results We identified a set of androgen-responsive genes that could serve as potential TAAs for PCa. In particular, we found transglutaminase 4 (Tgm4) to be highly expressed in prostate tumors that originate from luminal epithelial cells and only expressed at low levels in most extraprostatic tissues evaluated. Furthermore, elevated levels of *TGM4* expression in primary PCa tumors correlated with unfavorable prognosis in patients. In vitro and in vivo assays confirmed the immunogenicity of TGM4. We found that activated proinflammatory effector memory CD8 and CD4 T cells were expanded by monocyte-derived dendritic cell (moDCs) pulsed with TGM4 to a greater extent than moDCs pulsed with either PAP or prostate-specific antigen (PSA), and T cells primed with TGM4-pulsed moDCs produce functional cytokines following a prime/boost regiment or in vitro stimulation. An IgG antibody response to TGM4 was detected in 30% of vaccinated patients, while fewer than 8% of vaccinated patients developed antibody responses to PSA or prostate-specific membrane antigen (PSMA).

Conclusions These results suggest that TGM4 is an immunogenic, prostate-restricted antigen with the potential for further development as an immunotherapy target.

INTRODUCTION

Prostate cancer (PCa) remains a major public health concern among men worldwide. Although the majority of patients present with indolent, localized disease and are thus suitable candidates for active surveillance, a significant fraction of men present with higher-grade disease that warrants primary treatment with surgery or radiation.[1] Approximately 40% of patients with PCa recur after primary therapy and require further treatment with androgen-deprivation therapy (ADT), and the majority of recurrent patients eventually develop metastatic castration-resistant prostate cancer (mCRPC) for which treatment options are less effective.[2] Multiple immunological approaches have been studied as therapeutic options for castration-resistant prostate cancer (CRPC),[3] with limited success. In contrast to other tumor types, immunotherapy using immune checkpoint inhibitors (eg, anti-PD-1/PD-L1, and anti-CTLA-4) has shown limited responses in mCRPC to date.[4] Conversely, the ability of the only therapeutic Food and Drug Administration-approved PCa vaccine, sipuleucel-T, to extend survival[5–7] suggests that immunotherapy has potential in mCRPC. Due to the non-vital nature of the prostate gland, effective adaptive responses against prostate-restricted tumor-associated antigens (TAAs) such as prostatic acid phosphatase (PAP), prostate-specific antigen (PSA), prostate stem cell antigen (PSCA), transmembrane AMPA receptor regulatory protein (TARP), six transmembrane epithelial antigen of the prostate 1 (STEAP1), and prostate-specific membrane antigen (PSMA)

are feasible therapeutic targets for PCa,[3 4 8–10] although their clinical relevance remains unknown. The identification of novel prostate-restricted TAAs that induce de novo antitumor immune responses could guide the development of future immunotherapies. Here, we used a number of orthogonal approaches to identify transglutaminase 4 (TGM4) as a prostate-restricted TAA that is regulated in an androgen-dependent manner. The potential immunogenicity of this protein was verified using in vitro studies, as well as samples from a neoadjuvant clinical trial.[11]

MATERIALS AND METHODS

Patient samples

Serum samples from human patients with PCa were obtained with consent from patients treated with ADT alone (degarelix, 240 mg subcutaneous) or cyclophosphamide (200 mg/m^2 intravenous) followed by granulocyte-macrophage colony-stimulating factor [GM-CSF] gene transduced irradiated prostate cancer vaccine cells (GVAX) and ADT in a neoadjuvant trial (NCT01696877) at the Johns Hopkins Sidney Kimmel Comprehensive Cancer Center (Baltimore, Maryland, USA).[11 12] Men with high-risk localized PRAD, defined as clinical stage T1c-T3b, N0, M0 and a Gleason sum of ≥4+3 (grade group ≥3) in at least two cores were considered eligible if they were planning to undergo prostatectomy. All patients were required to have an Eastern Cooperative Oncology Group performance status of 0 or 1 and normal kidney, liver, and marrow function. Patients with nodal (N1) or distant (M1) metastases were excluded. Additional key exclusion criteria included prior immunotherapy or vaccine therapy for PCa, prior radiation, hormonal, or chemotherapy, autoimmune disease requiring corticosteroids, and known allergy to cyclophosphamide, GM-CSF, or granulocyte colony stimulating factor (G-CSF). All patients provided written, informed consent authorizing the collection of clinical data, serum and other biospecimens. Primary human peripheral blood mononuclear cells (PBMCs) from anonymous 35-year-old or older healthy male donors were acquired from the New York Blood Center.

Tissue acquisition and processing

All experiments using animals were performed according to protocols approved by the Institutional Animal Care and Use Committee at Columbia University Irving Medical Center. Wild-type mice of a hybrid 129/SvImJ and C57Bl/6J strain background at 12 months of age were used for immunofluorescence (IF) analyses. Briefly, lateral and dorsal prostate lobes, heart, bladder, kidney, liver, lung and spleen tissue were washed in ice-cold 1× phosphate-buffered saline (PBS) to remove excess blood, fixed in 10% formalin, and embedded in paraffin. Paraffin sections of 3–5 µm were cut using a microtome.

Protein expression

Protein expression for TGM4[13] and FOLH1/PSMA[14] in human tissues was queried using the Human Protein Atlas repository available online (http://www.proteinatlas.org).[15 16]

Antibody profiling

Phage-ImmunoPrecipitationSequencing (PhIP-Seq) antibody profiling was performed on 32 patients with PCa serum samples using a 90-aa peptide human proteome T7 phage display library as described previously.[17 18] Briefly, 2 µg of IgG, based on ELISA measurement of total IgG, was mixed with 2.5×10^{10} particle forming units of the 90-aa human peptidome library and incubated at 4°C overnight. IgG-bound phages were then immunoprecipitated using 20 µL of protein A magnetic Dynal beads and 20 µL of protein G coated Dynal beads (Invitrogen). After three bead washes, the library DNA inserts were amplified for 20 cycles of PCR using Herculase II Polymerase (Agilent). A second 20-cycle PCR reaction was performed in order to add sample-specific DNA bar codes and P5/P7 Illumina sequencing adapters. Sequencing was performed on an Illumina HiSeq 2500 in rapid mode (50 cycles, single-end reads).

Transcription profile of prostate luminal epithelial cells following androgen-induced regression/regeneration of the prostate

The transcription profile of Castration-Resistant Luminal Epithelial Cells (CRLECs) was evaluated as previously described.[19] Briefly, 12-week-old male Hoxb13-GFP mice carrying the *Hoxb13-rtTA* transgene and a tetracycline operator–histone 2B-green fluorescent protein, which results in GFP expression restricted to luminal epithelial Hoxb13$^+$ cells,[20] were castrated via bilateral orchiectomy. A cycle of prostate regression/regeneration was induced by allowing murine prostates to regress for 6 weeks to reach the fully involuted state. Mice were randomized to untreated, ADT or ADT-treated followed by testosterone repletion (ADT+TR) treatment groups. Testosterone was administered for 4 weeks for prostate regeneration by subcutaneous silastic implants yielding physiological levels of serum testosterone. All mice received 2 mg/mL of doxycycline (DOX; Sigma) in the drinking water to induce GFP expression[20] under the control of the luminal epithelial promoter, Hoxb13, 1 week prior to euthanization. CRLE cells were isolated based on their GFP$^+$ expression and CD45$^-$CD11b$^-$F4/80$^-$CD24$^+$CD49f^{int} status by flow sorting on a DakoCytomation MoFlo (online supplemental figure 1A, GSE171490). Differential gene expression was computed using the R limma package.[21] Transcriptional distribution of Log2-fold change (FC) for each gene in ADT versus untreated samples were normalized to z-scores. z-score values were obtained by scaling the data for each gene in each sample to (expression–mean expression across all genes)/(standard deviation of expression across all genes). The expression of androgen-responsive genes between ADT +TR/ADT samples was further evaluated by Log2 FC. Androgen-responsive gene signature was defined by the differential analysis of murine CRLECs from GFP$^+$ luminal prostate epithelial

cells comparing ADT versus untreated and ADT versus ADT +TR groups and included all differentially expressed genes with an ADT Log2 FC below the 0.005 percentile and a Bonferroni-corrected p<0.01 (online supplemental table 1), as well as a set of known androgen-responsive genes (*Klk1b8*, *Fkbp5*, *Nkx3.1*, and *Tmprss2*). Statistical analysis was performed in R,[22] and plotting was done using the ggplot2 R package V.3.1.0.[23]

IF staining

Antigen retrieval was performed on paraffin sections by boiling the slides in citrate-based antigen unmasking buffer for 45 min (Vector Labs H3300), then letting them gradually cool for 30 min. The slides were washed in 1× PBS twice to remove the buffer, then blocked in 5% animal serum for 1 hour. Primary antibody coating was performed by incubating the sections with Tgm4 (1:100; Invitrogen), Msmb (1:100; Abclonal), CK5 (1:500; Biolegend), and/or CK8/18 (1:250; developmental studies hybridoma bank: DSHB) primary antibodies overnight at 4°C. Then, the slides were washed twice with 1× PBS and incubated with Alexa Fluor secondary antibodies (Life Technologies) for 1 hour. Finally, the sections were washed twice in 1× PBS, stained with 4',6-diamidino-2-phenylindole (DAPI), and mounted (Vector Labs H-1200). Fluorescent images were acquired using a Leica TCS SP5 confocal microscope and analyzed using ImageJ, as described previously.[24]

Quantification of serum testosterone

Whole blood was collected from the tail vein and allowed to clot for 1 hour at 4°C. Serum was obtained by centrifuging (1000×*g* for 30 min) and collecting the supernatant. Sera were stored at −80°C prior to analysis. Testosterone concentration was determined by ELISA according to the manufacturer's instructions (Enzo, Farmingdale, New York, USA).

Transcriptional analysis across normal and cancer tissues

The expression profile of a subset of androgen-responsive genes was evaluated in publicly available dataset from mice (RIKEN FANTOM5)[25] and human (Genotype-Tissue Expression: GTEx)[26] normal tissues (prostate, brain, colon, liver, lung, skin, kidney, and salivary gland), as well as in lineage-marked benign or tumor prostate epithelial cells from transgenic mice (GSE39509).[27] For the later, we used RNA-seq data from luminal origin tumors of $Nkx3.1^{CreERT2/+}$, $Pten^{flox/flox}$, $R26R^{YFP/+}$ mice that were uninduced (benign), or at 3 months after induction. For tamoxifen induction, mice were administered 9 mg/40 g tamoxifen (Sigma) suspended in corn oil, or vehicle alone for negative controls, by oral gavage once daily for four consecutive days. In all presented boxplots, the medians for relative gene expression are shown. The 'hinges' represent the first and third quartiles. The whiskers are the smallest and largest values after exclusion of outliers (greater than the 75th percentile plus 1.5 times the interquartile [IQR], or less than 25th percentile minus 1.5 times the IQR). The expression levels of the complete signature of androgen-responsive genes, including *KLK3/PSA*, *FKBP5*, *NKX3.1*, and *TMPRSS2*, as well as the prostate-restricted TAAs: *STEAP1* and *TARP*, were also evaluated. The statistical analysis was performed in R[22] and plotting was done using the ggplot2 R package V.3.1.0.[23]

In addition, *TGM4* expression was plotted across human cancer types in TheCancer Genome Atlas (TCGA) database (n=11 284 samples), including 558 primary prostate adenocarcinomas (PRADs), and across an independent dataset that includes primary PRADs with clinical information on time to biochemical recurrence (n=218, GSE21032).[28] Biochemical recurrence was defined as a PSA of ≥0.2 ng/mL. Following radical prostatectomy, patients were followed up with history, physical exam, and serum PSA testing every 3 months for the first year, 6 months for the second year, and annually thereafter. The subset of primary PCa samples from this dataset was tested for association of *TGM4* expression with survival by Cox regression. Optimal cutpoint for *TGM4* selection was determined by maximizing the log-rank statistic using the R survminer package.[29]

Relative expression was quantified accordingly to the normalization methods used in the different publicly available databases analyzed here. RNASeq data from RIKEN FANTOM5 and GTEx were normalized to Log10 (transcripts per million: TPM), while RNASeq data from the GSE39509 dataset was normalized to fragments per kilobase million (FPKM) rather than TPM. Raw, un-normalized RNASeq data from TCGA were normalized to Log10 (TPM+1). Microarray data from GSE21032 was normalized with circular binary segmentation and analyzed with the statistical method RAE as previously described.[28]

Monocyte isolation and DC maturation

PBMCs from 10 anonymous healthy male donors ≥35 years of age obtained from the New York Blood Center were isolated using Lymphoprep and SepMate PBMC isolation tubes (STEMCELL Technologies). Untouched classical monocytes ($CD14^{+}CD16^{-}$) were then isolated from the PBMC fraction using magnetic beads following the manufacturer's instructions (Pan Monocyte Isolation Kit; Miltenyi Biotec). Following density gradient isolation, monocytes were resuspended in media containing IL-4 (1000 IU/mL) and GM-CSF (1000 IU/mL) at a concentration of 2×10^{6} cells /mL and cultured for 3 days. Cells were maturated for 2 days by adding lipopolysaccharides to a final concentration of 500 IU/mL (Sigma). moDCs were stimulated with 1 µg/mL of whole protein (TGM4, PAP, or PSA; Fisher Scientific and BioLegend) or viral peptide-libraries (CEFT or pp65; JPT Peptide Technologies) overnight before coculturing with autologous T cells.

Antigen-driven T-cell purification and expansion

Functional assays of protein-stimulated T-cell expansion were performed for 10 healthy male donors. On day

0, naïve T cells ($CCR7^+CD45RA^+$) were isolated from PBMCs by negative selection following the manufacturer's instructions (Naïve Pan T-Cell Isolation Kit; Miltenyi Biotec). Naïve T cells were cocultured with antigen-pulsed moDCs at a 1:10 ratio in cultured media (1:1 mix of AIM-V media and RPMI1640 (Thermo Fisher) with 10% human serum (Gemini Bio), 1% penicillin streptomycin (Life Technologies) and 1% GlutaMAX (Life Technologies)) supplemented with IL-7 (25 ng/mL, Peprotech). IL-2 (25 ng/mL, Peprotech) was added to the cultures 72 hours following priming of naïve T cells. Media were supplemented every 1–3 days with fresh culture media containing the same concentrations of IL-2 and IL-7. Every 10 days, cells were coincubated with a fresh set of antigen-pulsed moDCs. Cells were harvested and washed twice with PBS on day 30. As positive controls, cells were stimulated with a mixture of pathogen-associated peptides, CEFT pool and pp65 (JPT Peptide Technologies). Cells were stained for fluorescence-activated cell sorting (FACS) analysis 10 days after the last stimulation, and also stimulated with antigen-pulsed moDCs for 12 hours to evaluate the effect of activation markers on expanded T cells following stimulation.

Flow cytometry

Prior staining, cells were Fc-blocked with purified rat anti-mouse CD16/CD32 (Clone: 2.4G2, Becton Dickinson BD) for 15 min at room temperature (RT). Dead cells were discriminated using the LIVE/DEAD (L/D) fixable viability dye eFluor 506 dead cell stain kit (Thermo Fisher) and samples were stained for extracellular and intracellular markers. The following antibodies were used: CD3 (UCHT1), CD4 (A161A1), CD8 (SK1), CCR7 (3D12), CD45RA (MEM-56), CD69 (FN50), CD28 (CD28.2), CD27 (M-T271), CD161 (DX12), PD-1 (EH12.1), TIM3 (F38-2E2), CTLA-4 (L3D10), TBET (eBio4B10), GATA3 (TWAJ), RORg(t) (REA278), FOXP3 (PCH101), TCF1 (C63D9), EOMES (WD1928), IL-2 (MQ1-17H12), TNF-α (MAb11), IFN-γ (4S.B3), IL-4 (MP4-25D2), and Grz-B (N4TL33). Extracellular staining was performed at room temperature for 30 min. For intracellular staining, cells were fixed and permeabilized using BD Perm/Wash (BD Biosciences) at RT for 45 min. Cells were boosted for the final time with protein-pulsed moDCs for 12 hours to evaluate their activation status. For intracellular cytokine staining, cells were stimulated with PMA (50 ng/mL) and ionomycin (500 ng/mL) for 4 hours in the presence of protein transport inhibitor cocktail (eBiosciences). Gates for transcription factors were determined by fluorescence minus one (FMO) controls. Staining was visualized by fluorescence-activated cell sorting (FACS) analysis using a Cytek Aurora (Cytek Biosciences) and analyzed using FlowJo (Flowjo LLC) in combination with R packages uniform manifold approximation and projection (UMAP) V.0.2.0.0[30] and FlowSOM V.1.14.1.[31]

Multiparametric flow cytometry analysis

Following compensation, flow cytometry standard (FCS) files underwent standard preprocessing to remove debris, doublets and to enrich for live cells. Live, single cells were analyzed by manual gating and unsupervised computational methods in parallel.

For manual gating, T cells were identified based on CD3 expression followed by CD4 and CD8 extracellular markers using FlowJo V.10.6. Naïve, effector, CM, and EM subpopulations within CD4 and CD8 T cells were identified based on CD45RA and CCR7 expression. Antigen-driven T cells were quantified following three rounds of prime/boost autologous stimulation based on CD69, TBET, CD27, CD28, PD1 and TIM3, expression by manual gating.

Unsupervised computational analysis was performed separately for unstimulated and stimulated samples. In each case, 10,000 cells of postgated live, single $CD4^+$ or $CD8^+$ T cells from each of the 10 healthy donors were randomly selected using the DownSampleV3 plugin in FlowJo. Subsequently, unsupervised clustering was performed on the expression values of the activation and functional markers separately using the FlowSOM algorithm,[31] which uses a self-organizing map followed by hierarchical consensus metaclustering to detect cell populations. Default parameters and a predetermined number of 10 clusters were used. The median levels of the activation and functional markers across all cells per cluster were visualized in separate heatmaps. The subpopulations between clusters were based on the expression levels of activation and functional markers after applying the non-linear dimensionality reduction technique UMAP of the randomly selected cells using the R package UMAP for visualization of the multiparametric data.[30] The cells were colored according to their FlowSOM cluster membership.

ELISpot assays

TGM4-specific IFN-γ production by primed T cells was determined using following the manufactures recommendations (Mabtech). Briefly, T cells (1×10^4 cells/well) were stimulated at 37°C in 5% CO^2 for 48 hours with either TGM4-pulsed moDCs or unpulsed moDCs. Medium alone or anti-CD3 (100 ng/mL)+anti-CD28 mAb (5 ug/mL) were used as negative and positive controls, respectively. After revelation using BCIP/NBT solution, spots were counted using the Autoimmun Diagnostika GmbH iSpot reader (ELR08IFL). Results are presented as the mean of triplicate wells; numbers of spot-forming units are expressed for 10^4 cells.

Antibody analysis

PhIP-Seq data analysis was performed as described in the phip-stat package (https://github.com/lasersonlab/phip-stat). Reads were aligned to the phage library insert sequences using bowtie2[32] to generate a matrix of reads per million (RPM) values for each peptide in each sample (paired pre-treatment and post-treatment sera).

Using the phip-stat call-hits command with the '–fdr 0.05' option, we defined a set of statistically significant 'hits' where the RPM value was significantly higher than a set of control wells loaded with beads only. We also calculated the Log2 FC in post-treatment reactivity compared with pretreatment repertoire, with Laplace smoothing applied to avoid NA FC values from zero-inflated matrix (online supplemental figure 4A). We further analyzed only peptides with a post-treatment 'hit', such that RPM value is higher than the statistical baseline (online supplemental figure 4B). For PhIP-Seq Log2 FC analysis, RPM values were aggregated across peptides corresponding to each gene before computing FC for this analysis.

We generated a heatmap of sample-by-sample on-treatment versus pretreatment Log2 FC for the set of genes defined as androgen-responsive within patients with PRADs treated with ADT only or with GVAX followed by ADT treatment. This heatmap includes all androgen-responsive proteins profiled with at least one hit by PhIP-Seq. Relationship between immune response to androgen-responsive TAAs and biochemical recurrence-free survival among patients with PRAD in either treatment group was assessed by Kaplan-Meier curve with Cox regression p value as well as by Fisher exact test comparing frequency of immune response to any androgen-response gene in patients with recurrence versus patients without recurrence. All comparisons were performed in the R statistical computation environment.[22] Patients with positive Log2 FC for any androgen-responsive TAAs were considered to mount an immune response to any androgen-responsive TAAs. Androgen-responsive genes were defined in the differential analysis of murine CRLECs from GFP$^+$ luminal prostate epithelial cells, combined with a set of known androgen-responsive genes (*Klk1b8*, *Fkbp5*, *Nkx3.1*, and *Tmprss2*).

Immunoprecipitation of recombinant protein with patient sera

Using previously determined IgG concentrations (see Antibody profiling), ~2 µg of IgG was added with 1 µg of either recombinant human TGM4 (R&D Systems) or 1 µg of recombinant human ACPP/PAP (NovisBio), respectively, and brought to a total reaction volume of 100 µL with 1× PBS. Samples were incubated overnight at 4°C while rocking to facilitate specific antigen–antibody binding. Protein A and protein G conjugated metal beads (Invitrogen) were then added and allowed to incubate overnight at 4°C while rocking to facilitate protein A/G binding to the IgG-Fc region. Samples were washed 3× with 200 µL 1× PBS, placing the samples on a magnet for 5 min between each wash. Samples were then resuspended in 20 µL of H_2O and 20 µL of 2× Laemmli buffer+beta-mercaptoethanol (BME), for a total volume of 40 µL of 1× Laemmli buffer+BME. Samples were then boiled at 95°C for 10 min, then placed on a magnet, and the supernatant was then loaded on to a 4%–15% Mini-PROTEAN TGX Precast Protein gels (Bio-Rad) and run at 250 V for 25 min in 1× Tris/glycine/sodium dodecyl sulphate buffer. Protein was then transferred to a 0.2 m nitrocellulose membrane (Bio-Rad) using the Bio-Rad Trans-blot turbo transfer system. Membranes were then blocked in 5% BSA in 1×0.1% tween 20-tris-buffered saline (TBST) for 30 min at room temperature. Membranes were then exposed to either sheep–anti-human TGM4 primary (1:500; R&D Systems) or mouse anti-human PAP Primary (2 µg/mL; R&D Systems) overnight at 4°C while rocking. Membranes were washed 3× with 1×0.1% TBST for 5 min per wash. Membranes were then exposed to either horseradish peroxidase-conjugated anti-sheep IgG (1:10,000; for TGM4 membranes, Invitrogen) or Starbright 520-conjugated anti-mouse IgG (1:5000; for PAP membranes, Bio-Rad) for 1 hour at room temperature while rocking. Membranes were washed 3× with 1×0.1% TBST for 5 min per wash. TGM4 membranes were then exposed to 10 mL of substrate for 5 min before imaging using the ChemiDoc MP, set to auto-optimization. PAP membranes were imaged immediately following the wash step using the ChemiDoc MP, set to auto-optimization.

Band adjusted volume intensity was determined using Image Lab software (Bio-Rad, V.6.0.1 build 34, Standard Edition). Briefly, lanes were identified on each membrane using the autodetect feature and manually reviewed and modified to ensure accuracy. After lane identification, individual bands were identified using the autodetect feature, and similarly manually reviewed to ensure accuracy. After confirming the correct bands via molecular weight, adjusted volume intensity data were collected from the software and used for analysis. The adjusted volume intensity unit subtracts background signal from the final intensity unit.

Statistical analysis

Statistical analysis was performed using R V.3.6.1[22] or Prism V.7 (GraphPad). All statistical tests performed were two-sided with Bonferroni multiple-testing correction where applicable. Tests were considered statistically significant at p values of ≤0.05 (*), 0.01 (**), 0.001 (***) and 0.0001 (****).

RESULTS

Castration-resistant luminal epithelial cells (CRLECs) upregulate putative prostate antigens

Prior work showed that the murine prostate gland contains a population of CRLECs that is sufficient to regenerate prostatic architecture following consecutive rounds of androgen deprivation/repletion and which is the likely population of origin for PCa.[33] This population shares many features with castration-resistant prostate tumor cells.[34–36] To screen for potential prostate-restricted TAAs expressed by CRLECs, we quantified gene expression using a transgenic mouse model in which green fluorescent protein (GFP) expression is driven by the luminal-restricted *Hoxb13* promoter upon doxycycline (DOX) administration. Using cells sorted from these animals, we quantified the transcriptional profile of CRLECs following

an androgen deprivation/repletion cycle (figure 1A and online supplemental figure 1A,B, GSE171490).[19] We next defined a signature for androgen-responsive genes in our dataset as the intersection of genes differentially expressed when comparing untreated versus ADT-treated samples and ADT-treated versus ADT-treated followed by testosterone repletion (ADT+TR) samples. To derive this gene signature, we used an ADT Log2-fold change (FC) below the 0.005 percentile and a p value below 0.01 (figure 1B, online supplemental table 1). We then correlated each sample pair in terms of their expression of this gene signature, to quantify the degree of similarity between untreated and androgen-repleted samples (figure 1). Samples exposed to androgens showed a pairwise Pearson correlation of the androgen-responsive gene signature greater than 0.8 between samples from untreated animals and ADT-treated animals followed by TR, confirming the genetic program re-established by testosterone treatment (figure 1C). Conversely, the androgen-responsive gene signature in either untreated or testosterone-repleted animals correlated poorly with the signature in androgen-deprived animals, further confirming the relative specificity of this signature (figure 1C). Consistent with prior data,[37–42] we found that ADT downregulated the expression of several androgen-responsive genes including *Psca*, *Nkx3.1*, *Fkbp5*, and *Tmprss2* (figure 1B and online supplemental figure 1C,D). The relative androgen dependence of these transcripts is shown in figure 1D, with *Spink1*, *Msmb*, and *Tgm4* upregulated 3500-fold, 1900-fold, and 1500-fold, respectively, by androgen repletion, while androgen repletion upregulated the expression of *Psca* by 15-fold, *Nkx3.1* by 10-fold, *Fkbp5* by 5-fold, and *Tmprss2* by 2-fold. These results support a role for androgens in the regulation of *Spink1*, *Msmb*, and *Tgm4* genes as part of an androgen-responsive gene signature in CRLECs.

We next applied this signature to an independent dataset that we previously generated in which epithelial lineage-marked YFP$^+$ tumor cells from the prostates of transgenic mice expressing yellow fluorescent protein (YFP) under the luminal-restricted *Nkx3.1* promoter were profiled (GSE39509).[27] These data also showed *Tgm4* to be among the most highly overexpressed genes in prostate tumors with a luminal origin (figure 1E). Together, these finding support the notion that TGM4 is an androgen-responsive transcript expressed by prostate luminal epithelial cells, including CRLECs, in multiple datasets.

TGM4 shows prostate-restricted expression in human and murine datasets

To avoid inducing immunologically off-target effects, TAAs should have high expression in tumor tissue and minimal or undetectable expression in normal tissues. To evaluate which of the androgen-responsive genes are prostate tissue restricted, we interrogated two databases of gene expression from murine (RIKEN FANTOM5)[25] and human (GTEx)[26] normal tissues. We found low expression levels of *Defb50*, *Msmb*, *Sbp*, *Fkbp5*, *Spink1* and *Tgm4* in all murine extraprostatic tissues evaluated (figure 2A). Further immunostaining for Tgm4 and Msmb in benign prostate, heart, bladder, kidney, liver, lung and spleens tissues corroborated that Tgm4 expression is minimal in non-prostatic tissues. Msmb protein, however, is expressed in the spleen, heart, kidney, and lung, with the greatest expression observed in the bladder (figure 2B). Human data showed significant *FKBP5* and *SPINK1* expression in lung, liver, skin, colon, kidney, and salivary gland samples; these were greater than those for *TGM4* (figure 2C). Of note, *DEFB50*, *MSMB*, and *SBP* were not included in the human database. The expression levels of the established prostate-restricted targets *FOLH1/PSMA*, *KLK3/PSA*, and *PSCA* were high in human prostate; however, medium to low levels of expression were also observed in extraprostatic tissues. Specifically, brain, lung, liver, and kidney showed intermediate levels of *FOLH1/PSMA* expression at the RNA level (figure 2C) and high expression in kidney at the protein level (online supplemental figure 2), whereas TGM4 showed high specificity for prostate tissue. Detectable expression levels of *PSCA* and *ACPP/PAP* were found in human skin, lung and kidney tissues, and both *PSCA* and *ACPP/PAP* expression were significantly higher than that of *TGM4* in these extraprostatic tissues (figure 2C). Expression of additional prostate-restricted TAAs, including *TARP* and *STEAP1*, was also observed in both murine and human prostates, although at lower levels than *TGM4* (figure 2). While *STEAP1* expression was present in almost all the human tissues analyzed (lung, liver, skin, colon, kidney, and salivary gland), extraprostatic *TARP* expression was only observed in the lung, kidney, and salivary gland (figure 2C). In summary, these data indicate that TGM4 is generally not expressed at the message or protein level in non-prostate tissues, further supporting its investigation as a potential prostate-restricted TAA.

TGM4 expression correlates with PCa recurrence

We next studied the levels of *TGM4* expression in primary PCa and other human cancer types included in The Cancer Genome Atlas (TCGA). Consistent with data from lineage-marked murine luminal epithelial prostate tumors (figure 1E), the highest levels of *TGM4* expression were found in prostate adenocarcinomas (PRADs, figure 3A). We next tested whether *TGM4* expression in primary tumors is associated with disease progression in an independent dataset of PRADs (GSE21032). This analysis of differential *TGM4* expression revealed that patients whose primary tumors had higher expression of *TGM4* showed a significant decrease in time-to-PSA recurrence when compared with patients with low *TGM4* expression in their primary tumors using an optimal cutpoint determined by maximizing the long-rank statistic (figure 3B,C). These data support the notion that TGM4 expression may correlate with poor prognosis in PCa.[43]

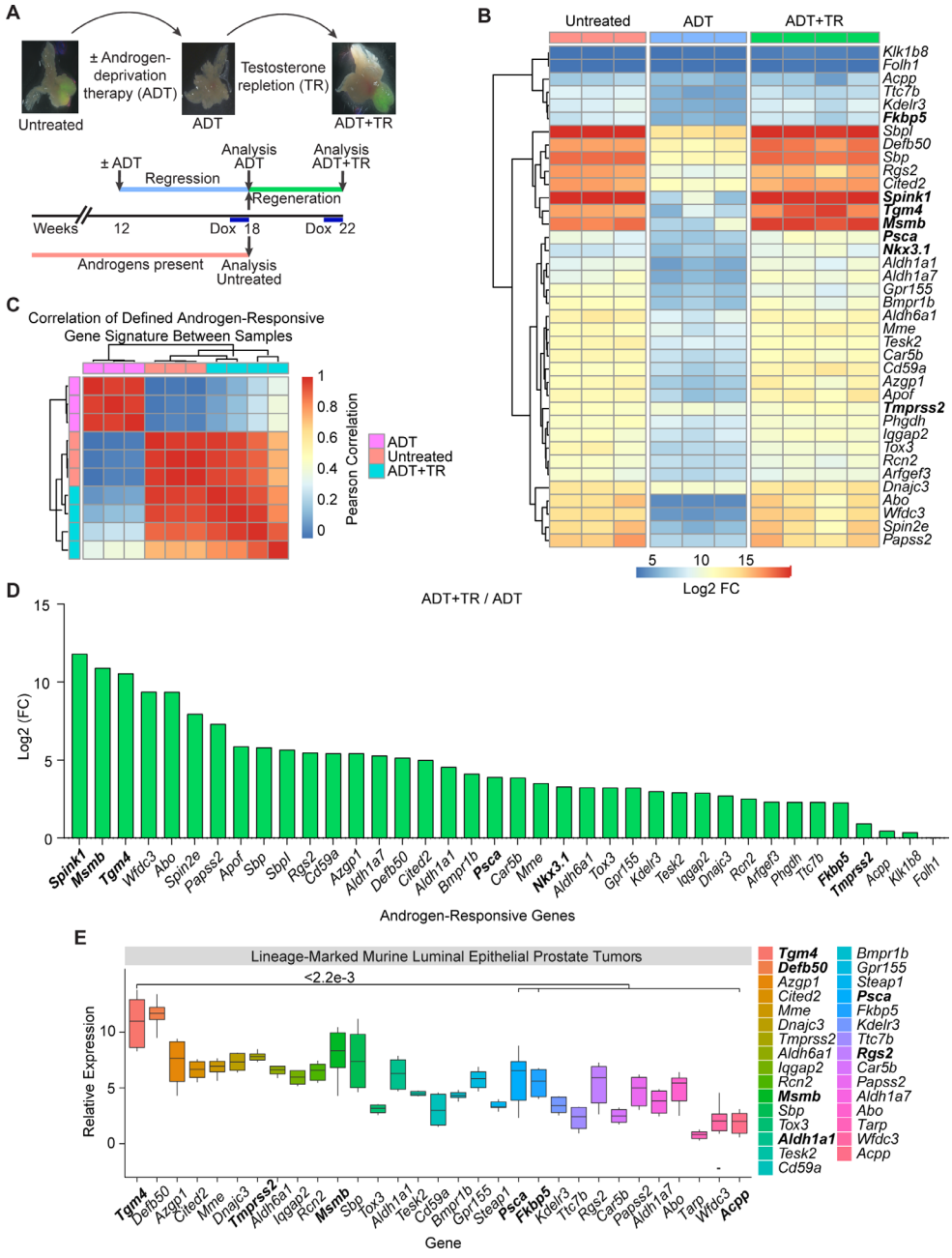

Figure 1 Putative prostate antigens are expressed by murine CRLECs in an androgen-dependent manner. (A) Schematic representation of androgen-induced prostate regression/regeneration in *Hoxb13-rtTA|TetO-H2BGFP* transgenic mice to model the cells of origin of prostate cancer (CRLECs). Top: representative fluorescent images of GFP$^+$ murine luminal epithelial cells to ADT and TR in murine prostates. Bottom: mice were treated with ADT (androgen depletion), testosterone pellets (androgen repletion), and DOX as indicated in the diagram and described in the Materials and methods section. (B) Differential expression profile of GFP$^+$ CRLECs isolated from the prostates of mice left untreated, treated with ADT, or treated with ADT plus androgen/TR (n≥3 per group). Heatmap showing androgen-responsive genes downregulated by ADT compared with both untreated and ADT+TR samples (n≥3 per group, GSE171490). (C) Heatmap showing pairwise Pearson correlation of androgen-responsive gene expression between CRLECs isolated from each mouse as described previously. Androgen-responsive gene signature (shown in B) with pairwise correlation between mice shown computed across all genes and annotated by treatment group. (D) Log2 FC in expression of androgen-responsive genes in GFP$^+$ CRLECs isolated from the prostates of mice treated with ADT in combination with androgen/TR compared with ADT alone. (E) Relative expression of androgen-responsive genes, as well as *Tarp* and *Steap1*, in prostate tumors originated from luminal epithelial cells isolated from lineage-marked *Nkx3.1*$^{CreERT2/+}$, *Pten*$^{flox/flox}$, *R26R-YFP*/+ transgenic mice (n≥5, GSE39509).[27] Boxplots of Log10 (FPKM) normalized gene expression are shown (n=6). (B,D) Selected genes for each comparison are defined as genes with ADT Log2 FC below the 0.005 percentile and p<0.01, in addition to a set of known androgen-responsive genes from the literature (*Acpp*, *Klk1b8*, *Fkbp5*, *Nkx3.1*, *Tmprss2*, and *Folh1*). Wilcoxon test was used for statistical analysis between *Tgm4* and each indicated gene; p values are displayed. ADT, androgen-deprivation therapy; CRLEC, castration-resistant luminal epithelial cell; DOX, doxycycline; FC, fold change; TetO-H2BGFP, tetracycline operator–histone 2B-green fluorescent protein; *Tgm4*, transglutaminase 4; TR, testosterone repletion.

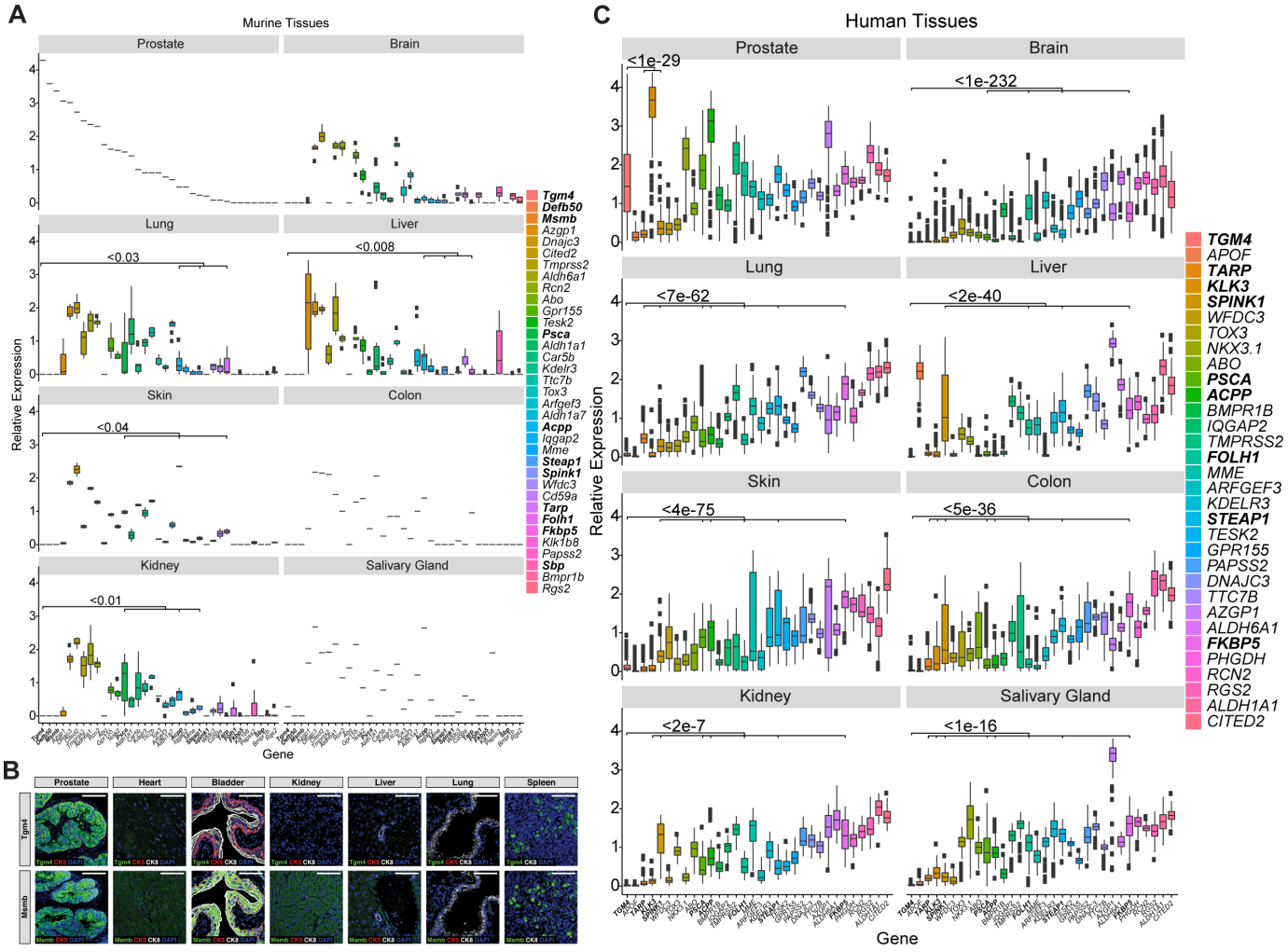

Figure 2 Expression of putative prostate antigens is restricted to the prostate in both mouse and humans. (A) Relative expression of androgen-responsive genes, as well as *Tarp* and *Steap1*, across normal murine tissues. Boxplots of Log10 (TPM) normalized gene expression in prostate (n=1), brain (n=9), colon (n=1), liver (n=10), lung (n=9), skin (n=2), kidney (n=7), and salivary gland (n=1) from RIKEN FANTOM5 are shown, and genes are ordered by decreasing expression in murine prostate. (B) IF images of selected markers in adjacent sections from indicated mouse tissues—the prostate lobes shown are dorsal prostate lobes for Tgm4 and lateral prostate lobes for Msmb. Scale bars indicate 50 µm. (C) Relative expression of androgen-responsive genes, as well as *TARP* and *STEAP1*, across normal human tissues. Boxplots of Log10 (TPM) normalized gene expression in prostate (n=152), brain (n=1671), colon (n=507), liver (n=175), lung (n=427), skin (n=1203), kidney (n=45), and salivary gland (n=97) from GTEx are shown. Wilcoxon test was used for statistical analysis between TGM4 and each indicated gene; p values are displayed. GTEx, Genotype-Tissue Expression; IF, Immunofluorescence; *TGM4*, Transglutaminase 4.

Prostate-restricted TAA TGM4 induces an in vitro CD8$^+$ T-cell response when presented by autologous monocyte-derived DCs

To further determine whether TGM4 could serve as a potentially targetable TAA, we tested whether T-cell responses to TGM4 could be induced in vitro. For these experiments, naïve T cells purified from the peripheral blood mononuclear cells (PBMCs) of healthy male donors (n=10) were individually cocultured with autologous monocyte-derived dendritic cells (moDCs) pulsed with either full-length protein TAAs (PAP, PSA, and TGM4) or a positive control comprised of a viral peptide-library (pp65 and CEFT - Cytomegalovirus, Epstein-Barr virus, Influenza virus and Clostridium tetani) in a 30-day culture system (figure 4A,B). To analyze responses, we used multiparametric flow cytometry to quantify antigen-driven expansion of CD8 T cells and identified eight distinct populations using self-organizing maps for clustering analysis (FlowSOM; figure 4C,D). Of these, Pop6 appeared to represent central memory (CM) CD8 T cells and Pop4 naïve CD8 T cells (figure 4D). Antigen-driven expansion of effector memory (EM) CD8 T cells was reflected by Pop5, which upregulated the self-renewing transcription factor TCF1 and the interleukin (IL)-7 receptor (CD127) (figure 4D). The expansion of both activated CM and EM CD8 T cells was confirmed post-stimulation (figure 4E,F). Importantly, activated (CD69$^+$) CD27$^+$CD28$^+$ memory CD8 T cells expanded to a significantly greater degree in cocultures with TAA-pulsed moDCs than with the positive control viral antigens

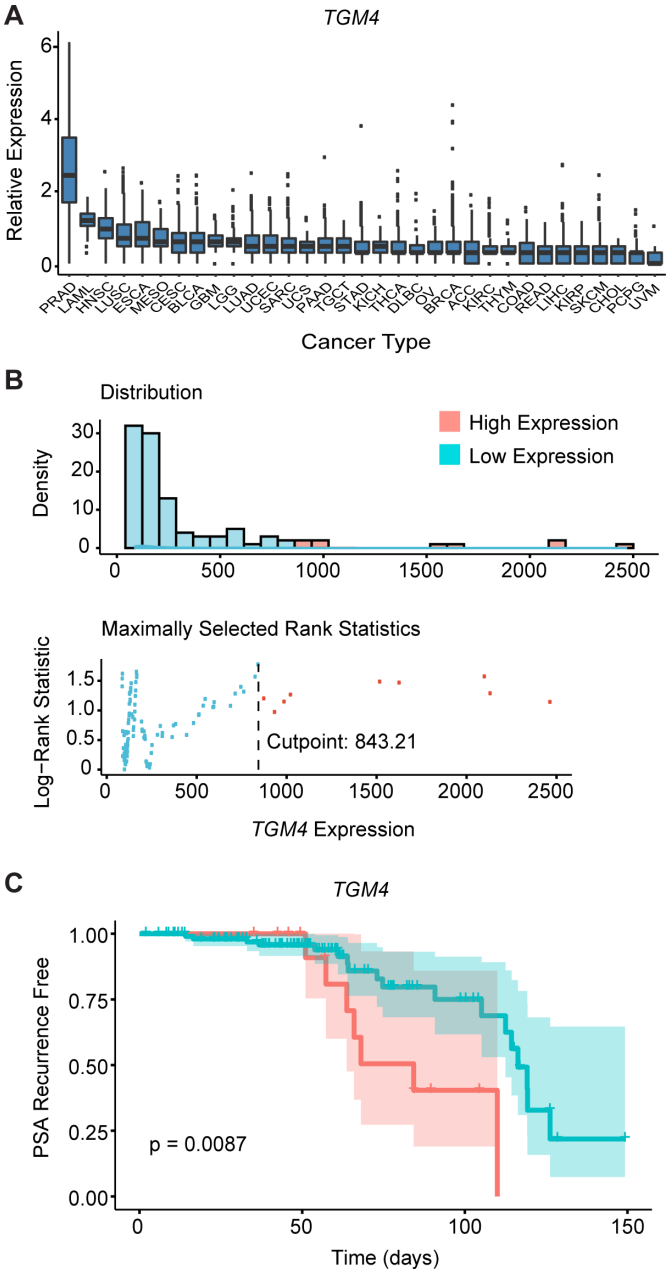

Figure 3 TGM4 expression is maintained by prostate tumor cells. (A) Relative expression of *TGM4* across human cancer types in TCGA database, including 558 primary PRADs.[73] Boxplots of Log10 (TPM) normalized gene expression are shown, with cancer types ordered by decreasing *TGM4* expression. (B) Optimal cutpoint for *TGM4* expression. Top: distribution of *TGM4* expression across primary PRADs (n=218, GSE21032).[28] Bottom: the overall log-rank p value for *TGM4* expression is plotted. A vertical line is drawn at the optimal cutpoint of 843.21. (C) Kaplan-Meier curves comparing biochemical recurrence-free survival of patients with PRADs, with log-rank p value reported from multiple Cox regression of biochemical recurrence-free against *TGM4* expression levels (high *TGM4*, n=24; low *TGM4*, n=107). Biochemical recurrence was determined as an increase in PSA serum levels of ≥0.2 ng/mL on two occasions as described in the Materials and methods section. PRAD, prostate adenocarcinoma; TCGA, The Cancer Genome Atlas; *TGM4*, Transglutaminase 4.

(figure 4E,F). Accordingly, higher percentages of CM and EM expressed PD-1 and TIM3 when stimulated by TAA-loaded moDCs; in this setting, these molecules likely represent early activation markers rather than markers of exhaustion (figure 4G). Additional manual gating for the EM CD8 T-cell population expressing the proinflammatory transcription factor TBET (Pop 1, figure 4D) was performed (figure 4H). Here, we found that TGM4-pulsed moDCs drove the expansion of TBET$^+$-activated EM CD8 T cells to a significantly greater extent than PAP-pulsed and PSA-pulsed moDCs, but to a degree similar to the viral control antigens, CEFT and pp65 (figure 4I). Furthermore, TBET$^+$ activated EM CD8 T cells primed with TGM4-pulsed moDCs produced canonical effector cytokines (IL-2, tumor necrosis factor alpha (TNF-α), interferon gamma (IFN-γ), and granzyme-B) following stimulation (figure 4J,L). ELISpot assays confirmed activation, with significant IFN-γ production noted after an in vitro prime/boost regimen with TGM4-pulsed moDCs (online supplemental figure 3). Taken together, these findings show that donor-derived naïve CD8 T cells expand and differentiate following TGM4 recognition and suggest that this prostate-restricted TAA could potentially be more immunogenic than either PAP or PSA.

Prostate-restricted TAA TGM4 induces an in vitro CD4$^+$ T-cell response when presented by autologous monocyte-derived DCs

We next performed analyses similar to those mentioned previously for CD4 T cells. As shown in figure 5A,B, FlowSOM clustering showed ten distinct populations of antigen-driven expanded CD4 T cells. Most of these clusters were observed in all antigen-driven expanded CD4 T cells (with the exception of Pop 5; figure 5A). Of these, Pop9 appears to represent CM CD4 T cells and Pop6 naïve CD4 T cells (figure 5B). In terms of CM and EM CD4 T cells, we found that stimulation by TAA-pulsed moDCs increased the proportion and percentages of activated (CD69$^+$) CD27$^+$CD28$^+$ CM CD4 T cells to a significantly greater extent than did coculture with the positive control viral antigens (figure 5D). Accordingly, higher percentages of CM and EM expressed the activation markers PD-1 and TIM3 when stimulated with TAAs (figure 5E). Additional manual gating for the EM CD4 T-cell population expressing the proinflammatory transcription factor TBET (Pop 0, figure 5B) was performed (figure 5F,G). Here, we observed TGM4-pulsed moDCs increased expansion of TBET$^+$-activated EM CD4 T cells to a greater degree than PAP-pulsed or PSA-pulsed moDCs, with levels similar to those from positive control viral antigens, CEFT and pp65 (figure 5H). Furthermore, TBET$^+$-activated EM CD4 T cells primed with TGM4-pulsed moDCs produce canonical proinflammatory cytokines (IL-2, TNF-α, and IFN-γ, but not IL-4) following stimulation (figure 5I,K). These data support the notion that TGM4 can potentially drive proimmunogenic CD4 T-cell responses in addition to the CD8 responses shown previously.

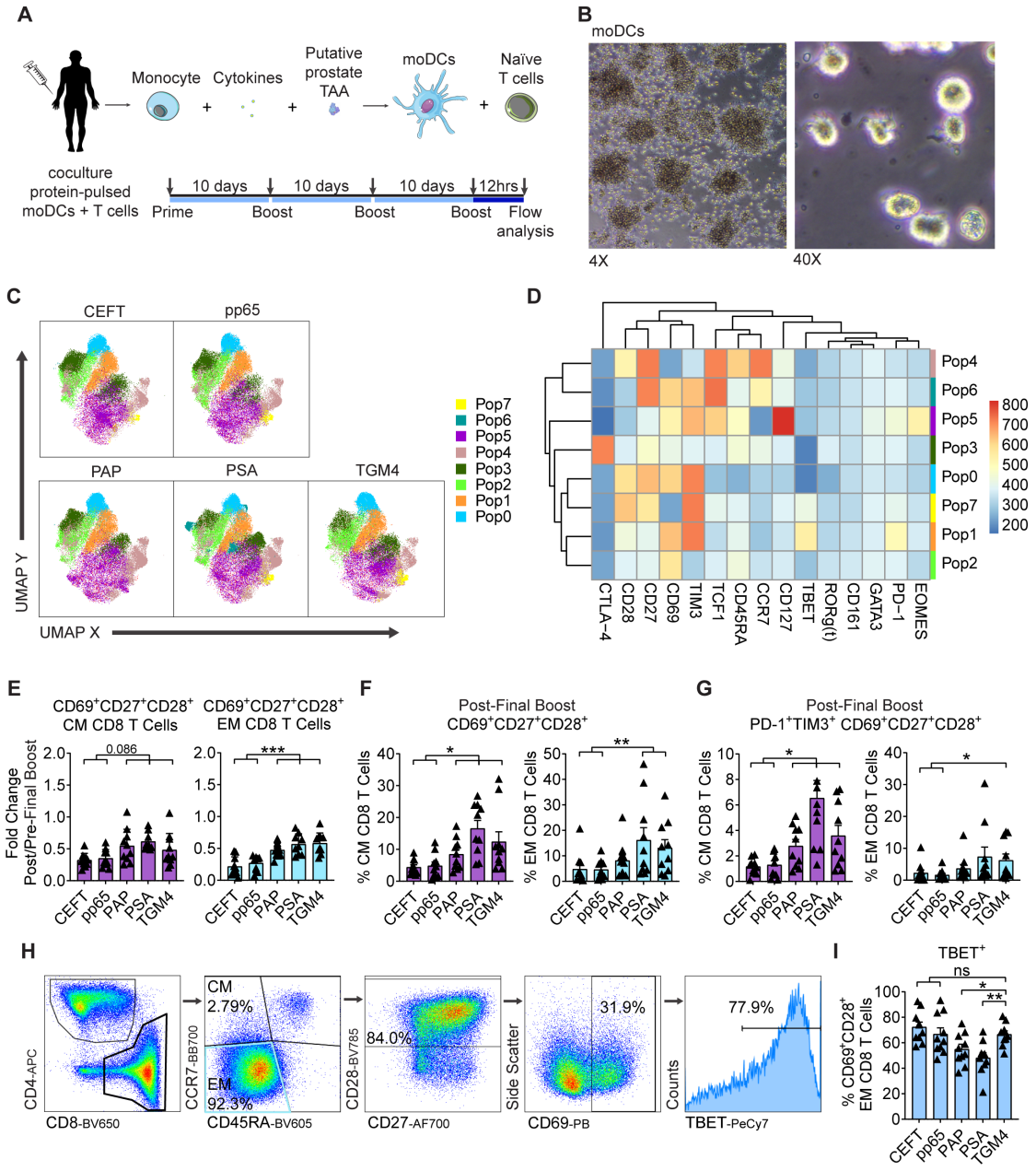

Figure 4 TGM4 induces CD8 T-cell activation and expansion in vitro. (A) Schematic representation of the 30-day prime/boost coculture of autologous moDCs and naïve T cells. (B) Representative images of differentiated moDCs. 4X (left) and 40X (right) magnification. (C) Differential expression of functional markers on expanded populations of CD8 T cells following coculture with autologous protein-pulsed moDCs. Heatmap showing unsupervised clusters determined with the FlowSOM algorithm as described in the Materials and methods section. (D) Expanded CD8 T-cell populations defined by FlowSOM (in C) were projected onto UMAP space as described in the Materials and methods section. Colors correspond to FlowSOM populations. (E) Fold change on activated $CD69^+CD27^+CD28^+$ EM CD8 T cells (left) and CM T cells (right) following the last 12-hour stimulation in expanded T cells. (F) Activated $CD69^+CD27^+CD28^+$ cells as a percentage of EM CD8 T cells (left) and CM CD8 T cells (right) following in vitro expansion (as in E). (G) $PD1^+TIM3^+$ $CD69^+CD27^+CD28^+$ cells as a percentage of EM CD8 T cells (left) and CD8 T cells (right) following in vitro expansion (as in E). (H) Gating strategy used to manually analyze $TBET^+$ in activated $CD69^+CD28^+$ EM CD8 T cells defined as $CCR7^-CD45RA^-$ following coculture with autologous protein-pulsed moDCs. (I) $TBET^+$ cells as a percentage of activated $CD69^+CD28^+$ EM CD8 T cells in expanded T cells (gated as in C). (J) Schematic representation of priming of naïve T cell with autologous TGM4-pulsed moDCs stimulated with PMA/ionomycin 4 hours prior analysis by flow cytometry. (K) Gating strategy used to manually analyze cytokine production on activated $TBET^+CD69^+CD28^+$ EM CD8 T cells defined as $CCR7^-CD45RA^-$ following coculture with autologous TGM4-pulsed moDCs stimulated with PMA/ionomycin. (l) Cytokine production as a percentage of activated $TBET^+CD69^+CD28^+$ EM CD8 T cells in expanded T cells (gated as in K). Unpaired t-tests performed; *p≤0.05, **p≤0.01, ***p≤0.001. CM, central memory; EM, effector memory; IFN-γ, interferon gamma; IL, interleukin; moDC, monocyte-derived dendritic cell; ns, not statistically significant; PAP, prostatic acid phosphatase; PSA, prostate-specific antigen; CEFT, Cytomegalovirus, Epstein-Barr virus, Influenza virus and Clostridium tetani; TAA, tumor-associated antigen; TGM4, transglutaminase 4.

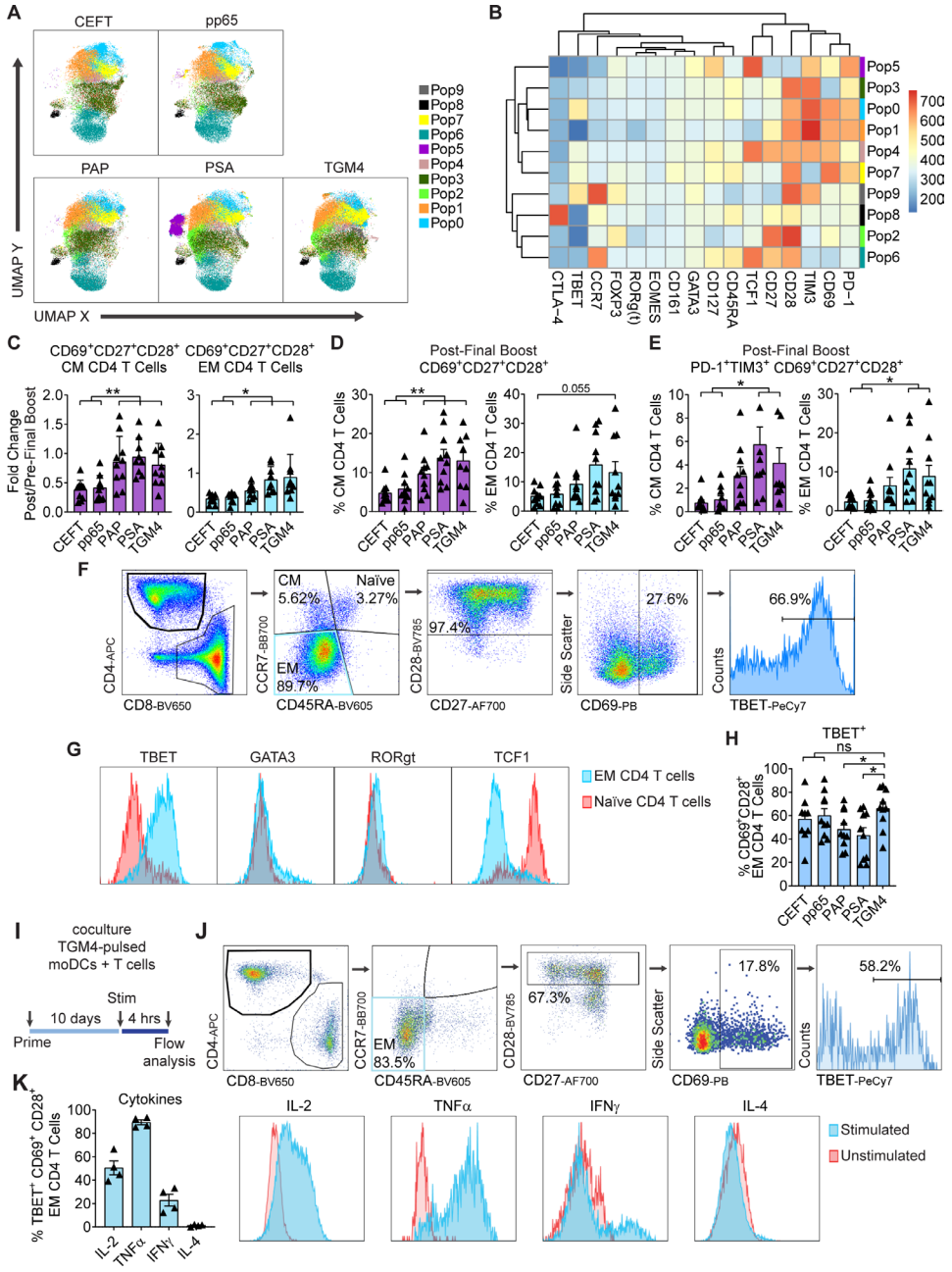

Figure 5 TGM4 induces CD4 T-cell activation and expansion in vitro. (A) Differential expression of functional markers on expanded populations of CD4 T cells following coculture with autologous protein-pulsed moDCs. Heatmap showing unsupervised clusters determined with the FlowSOM algorithm as described in the Materials and methods section. (B) Expanded CD4 T-cell populations defined by FlowSOM (in A) were projected onto UMAP space as described in the Materials and methods section. Colors correspond to FlowSOM populations. (C) Fold change on activated $CD69^{+}CD27^{+}CD28^{+}$ EM CD4 T cells (left) and CM CD4 T cells (right) following the last 12 hours of stimulation in expanded T cells. (D) Activated $CD69^{+}CD27^{+}CD28^{+}$ cells as a percentage of EM CD4 T cells (left) and CM CD4 T cells (right) following in vitro expansion (as in C). (E) $PD1^{+}TIM3^{+}$ $CD69^{+}CD27^{+}CD28^{+}$ cells as a percentage of EM CD4 T cells (left) and CM CD4 T cells (right) following in vitro expansion (as in C). (F) Gating strategy used to manually analyze $TBET^{+}$ in activated $CD69^{+}CD28^{+}$ EM CD4 T cells defined as $CCR7^{-}CD45RA^{-}$ following coculture with autologous protein-pulsed moDCs. (G) Representative histograms of expression levels of functional transcription factors determined by flow cytometry in expanded EM and naïve CD4 T cells. (H) $TBET^{+}$ cells as a percentage of activated $CD69^{+}CD28^{+}$ EM CD4 T cell in expanded T cells (gated as in F). (I) Schematic representation of priming of naïve T cell with autologous TGM4-pulsed moDCs stimulated with PMA/ionomycin 4 hours prior analysis by flow cytometry. (J) Gating strategy used to manually analyze cytokine responses on activated $TBET^{+}CD69^{+}CD28^{+}$ EM CD4 T cells defined as $CCR7^{-}CD45RA^{-}$ following coculture with autologous TGM4-pulsed moDCs stimulated with PMA/ionomycin. (K) Cytokine production as a percentage of activated $TBET^{+}CD69^{+}CD28^{+}$ EM CD4 T cells in expanded T cells (gated as in I). Unpaired t-tests performed; *p≤0.05, **p≤0.01. CEFT, cytomegalovirus, Epstein-Barr virus, influenza virus and clostridium tetani; CM, central memory; EM, effector memory; IFN-γ, interferon gamma; IL, interleukin; moDC, monocyte-derived dendritic cell; ns, not statistically significant; PAP, prostatic acid phosphatase; PSA, prostate-specific antigen; TGM4, transglutaminase 4.

Patients with PCa develop a humoral response to TGM4 after treatment with granulocyte-macrophage colony-stimulating factor [GM-CSF] gene transduced irradiated prostate cancer vaccine cells (GVAX)

Given the induced CD4 T-cell responses to TGM4 observed in vitro (figure 5), we hypothesized that patients with PCa might leverage CD4 T-cell help to mount an IgG antibody response against this prostate-restricted TAA. To address this question, we analyzed pre-treatment and post-treatment sera from patients with localized prostate tumors treated with either ADT (n=14) or ADT plus a cell-based PCa vaccine (GVAX+ADT, n=13) in the neoadjuvant setting[11] (figure 6A). To profile antibody responses, we used Phage-ImmunoPrecipitation

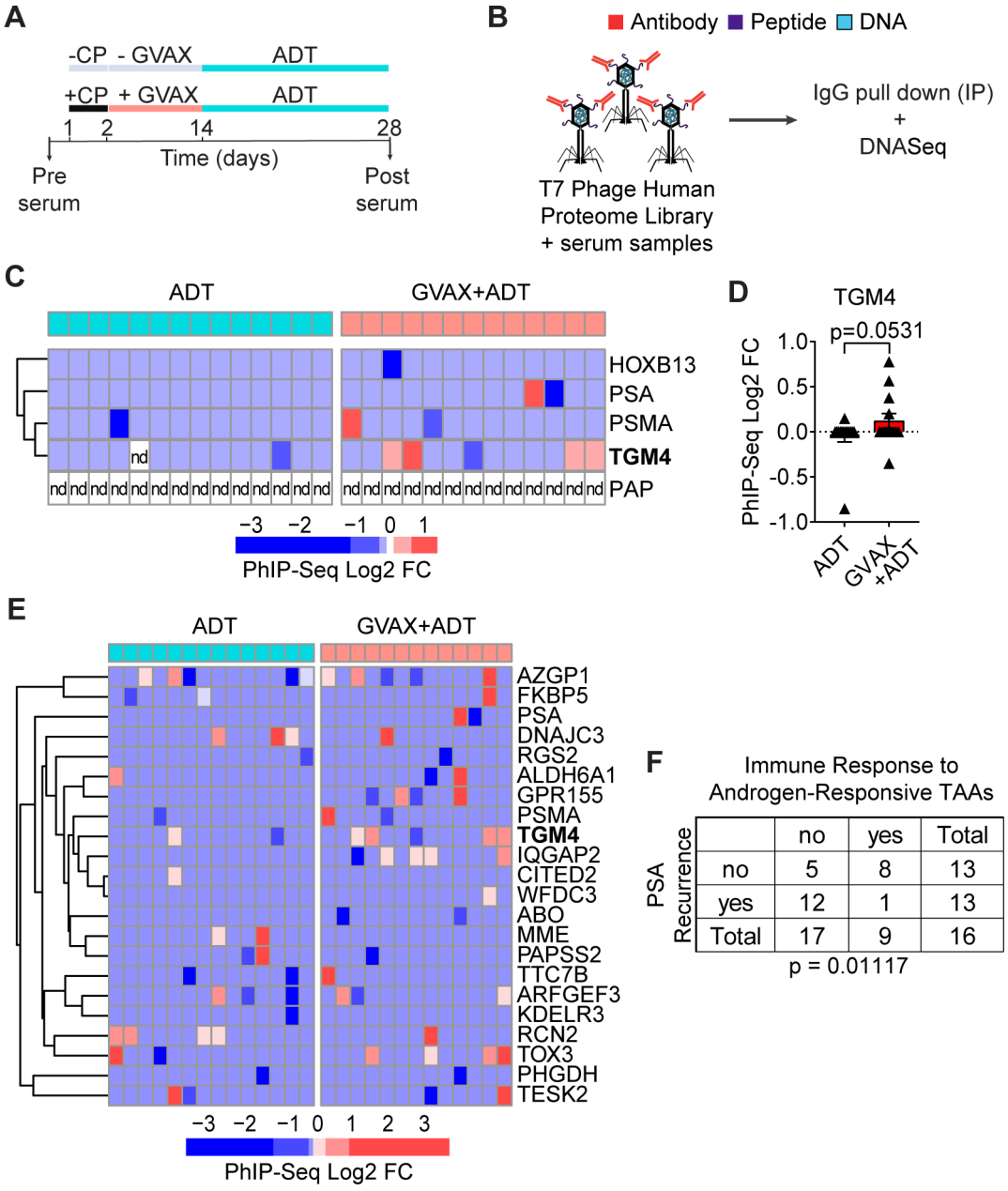

	no	yes	Total
no	5	8	13
yes	12	1	13
Total	17	9	16

Figure 6 GVAX vaccination induces antibody responses against TGM4 in patients with prostate cancer. (A) Schematic representation of the treatment paradigm of patients with PRAD treated with ADT alone or CP followed by GVAX and ADT in a neoadjuvant trial (NCT01696877). (B) Schematic diagram of the PhIP-Seq assay. (C) Heatmap of antibody binding to selected prostate-restricted TAAs determined as described in the Materials and methods section. (D) Antibody response to TGM4 across patients with PRAD (treated as in A). (E) Heatmap of antibody binding to androgen-responsive antigens determined as described in figure 2. (F) Table summarizing responses for ADT only and GVAX followed by ADT treatment groups. Fisher's exact test shows significant over-representation of immune response to androgen-responsive TAAs in the set of patients without biochemical recurrence. ADT, androgen-deprivation therapy; CP, cyclophosphamide; FC, fold change; GVAX, granulocyte-macrophage colony-stimulating factor [GM-CSF] gene transduced irradiated prostate cancer vaccine cells; nd, not detected; PhIP-Seq, Phage-ImmunoPrecipitation sequencing; PRAD, prostate adenocarcinoma; TAA, tumor-associated antigen; TGM4, transglutaminase 4.

Sequencing (PhIP-Seq),[44] focusing on IgG antibody responses. For these assays, serum samples pre-treatment and post-treatment were used to immunoprecipitate a T7 phage-displayed library expressing overlapping 90-aa peptides covering 29 371 human open reading frames (figure 6B).[44 45] Fewer than 8% of vaccinated patients developed antibody responses to PSA or PSMA and antibodies against PAP were not detected in any patient studied (figure 6C,D). By contrast, approximately 30% of vaccinated patients developed an antibody response to TGM4. To validate the presence of antibodies against TGM4 post-vaccination and address the absence of antibodies against PAP, we performed immunoprecipitation experiments using either TGM4 or PAP recombinant protein and patient sera pre-vaccination and post-vaccination—followed by western blotting. Indeed, we were able to detect antibodies against both TGM4 and PAP in both pre-vaccination and post-vaccination samples. Interestingly, using this strategy that preserves protein structure, we observed a numerical increase in post-vaccination antibody responses to TGM4 but not PAP (online supplemental figure 4C,D). Further, antibody responses to TGM4 and other androgen-responsive TAAs correlated with PSA recurrence in this dataset (figure 6E,F). These results suggest that vaccine-induced responses to androgen-responsive TAAs may have clinical relevance in patients with PCa.

DISCUSSION

The clinical activity of a PCa vaccine based on PAP-loaded autologous moDCs (sipuleucel-T) highlights the potential of immunotherapy to enhance de novo antitumor immune responses to prostate-restricted TAAs. Despite the clinical utility of PAP as an immunological target, responses to this prostate-restricted TAA are heterogeneous.[46–50] Other prostate-restricted TAAs such as PSA, PSCA, and PSMA have also shown intriguing results in preclinical studies and are currently under investigation in clinical trials (NCT03089203, NCT04053062, NCT03873805, and NCT02744287).[51–54] However, the identification of novel prostate-restricted immunological targets remains an unmet need. Here we show that the putative cell-of-origin for PCa,[55] a subpopulation of epithelial cells surrounding the ductal lumen that survive after androgen deprivation—known as CRLECs, express high levels of prostate specific *Tgm4* in an androgen dependent manner. Our findings are in agreement with our recent study that histologically located Tgm4 at the protein level to luminal cells in the anterior and dorsal lobes of mouse prostates,[24] as well as with previous in vitro studies suggesting *TGM4* may be responsive to androgens in a human PCa cell line.[37 56] Although Tgm4 is expressed in benign prostate tissue, the non-vital nature of the prostate gland makes it a feasible target for immunotherapy in patients with recurrent disease after primary therapy with radiation or surgery. In addition, we found that *Tgm4* expression is increased in prostate tumors originating from luminal epithelial cells. Furthermore, the relatively low levels of TGM4 expression observed in brain, colon, liver, lung, skin, kidney, and salivary gland suggest that targeting TGM4 might be associated with fewer off-target immune-related adverse events than other potential TAAs.

Of note, there has been some controversy regarding TGM4 expression in prostate tumor lesions as compared with benign prostate tissue, with some studies reporting TGM4 expression in tumor lesions to be lower[57–59] or higher[43] than that in benign prostate tissue. At the message level, *TGM4* expression has been reported to be reduced in PRAD and metastatic PCa tissue compared with the benign tissue by qPCR[57] and northern hybridization[58]; however, further studies demonstrated that only one of four *TGM4* splice variants (4 L) is lost in PCa samples.[60] At the protein level, two independent immunohistochemistry analyses of prostate tissue microarray slides revealed that TGM4 expression was higher in benign prostatic tissue when a polyclonal antibody was used,[59] but higher in PRADs when evaluated with a monoclonal antibody.[43] Thus, potential discrepancies could possibly be explained by the reagents used in each study. In line with a potential role for TGM4 in disease progression,[61 62] our results suggest that TGM4 expression is associated with decreased time to recurrence.

To understand whether TGM4 expression was able to induce an antigen-driven immune response, we evaluated the immunogenicity of TGM4 and several additional prostate-restricted TAAs in functional assays with pulsed moDCs presenting one of the three human proteins (TGM4, PAP, or PSA) to autologous naïve T cells from healthy male donors. Using these tools, we found that proinflammatory activated $TBET^{+}$ EM CD8 and CD4 T cells were expanded by TGM4-pulsed moDCs to a greater extent than PAP-pulsed and PSA-pulsed moDCs in healthy male donors. These studies were notable in that they support the notion that a TGM4 targeted vaccine could potentially induce T-cell immunity.

We also found that an IgG antibody response to TGM4 was detected in a fraction of patients with PCa treated with GVAX in a neoadjuvant trial. Those data further support the potential for antigen-driven CD4 T-cell responses to TGM4, since CD4 T help is required for antibody class switching to IgG. This finding is in line with the modest improvement in time-to-PSA progression observed in this trial,[11] an improvement which was not associated with an increase in tumor-infiltrating CD8 T cells. Further supporting the immunogenicity of TGM4, work from others showed that autoantibodies were found in 100% of *Aire*-deficient and in 22% of non-obese diabetic male mice that spontaneously developed prostatitis, but not in female mice.[63] Interestingly, several other members of the transglutaminase family have also been identified as immune targets in inflammatory and autoimmune

disorders.[64–66] *Aire*-deficient mice with antibodies targeting Tgm4 lack production of Tgm4, suggesting that Tgm4-expressing cells may be destroyed by an autoimmune reaction.[63] Further, the development of antibodies targeting Tgm4 was only observed postpuberty,[63] which parallels the androgen-responsive regulation we observed and implies peripheral antigen recognition in the absence of central tolerance.

In summary, these studies support further evaluation of TGM4 as a prostate-restricted TAA. Given the immunosuppressive nature of the tumor microenvironment in PCa,[3 67–72] it is likely that vaccine-induced responses against TGM4 may not be sufficient alone for an effective antitumor response. Instead, targeted vaccines may need to be administrated in combination with other therapies targeting the recruitment and accumulation of regulatory T cells and/or myeloid-derived suppressive cells. Future studies evaluating TGM4 as a putative target antigen in mCPRC are required to explore these issues.

Author affiliations
[1]Department of Pathology, Johns Hopkins University School of Medicine, Baltimore, Maryland, USA
[2]Columbia Center for Translational Immunology, Columbia University Irving Medical Center, New York, New York, USA
[3]Bloomberg~Kimmel Institute for Cancer Immunotherapy, Johns Hopkins Medicine Sidney Kimmel Comprehensive Cancer Center, Baltimore, Maryland, USA
[4]Current: Molecular Pathogenesis Program, The Kimmel Center for Biology and Medicine of the Skirball Institute, New York University School of Medicine, New York, NY, USA
[5]Department of Genetics and Development, Columbia University Irving Medical Center, New York, New York, USA
[6]Herbert Irving Comprehensive Cancer Center, Columbia University Irving Medical Center, New York, New York, USA
[7]Department of Medicine, Columbia University Irving Medical Center, New York, New York, USA
[8]Department of Systems Biology, Columbia University Irving Medical Center, New York, New York, USA
[9]Department of Urology, Columbia University Irving Medical Center, New York, New York, USA
[10]Department of Molecular Pharmacology and Therapeutics, Columbia University Irving Medical Center, New York, New York, USA
[11]Department of Genetics and Genomic Sciences, Icahn School of Medicine at Mount Sinai, New York, New York, USA
[12]Department of Oncology, Johns Hopkins Medicine Sidney Kimmel Comprehensive Cancer Center, Baltimore, Maryland, USA
[13]Division of Hematology Oncology, Columbia University Irving Medical Center, New York, New York, USA
[14]Division of Immunology, Department of Pathology, Johns Hopkins University School of Medicine, Baltimore, Maryland, USA
[15]Institute of Cell Engineering, Johns Hopkins University, Baltimore, Maryland, USA
[16]Divisions of Human Biology and Clinical Research, Fred Hutchinson Cancer Research Center, Seattle, Washington, USA

Twitter Zoila A Lopez-Bujanda @ZoilaBujanda and Alexandros Papachristodoulou @Alexandros_P

Acknowledgements We thank C Abate-Shen for her assistance in facilitating this collaboration, N Chowdhury, C R Ager, C S Spina, and S L Reiner for discussion and insightful comments, M G Chaimowitz for administrative assistance, and Z J Kerner for his help revising the manuscript. The Genotype-Tissue Expression (GTEx) Project was supported by the Common Fund of the Office of the Director of the National Institutes of Health, and by National Cancer Institute (NCI), National Human Genome Research Institute (NHGRI), National Heart, Lung, and Blood Institute (NHLBI), National Institute on Drug Abuse (NIDA), National Institute of Mental Health (NIMH), and National Institute of Neurological Disorders and Stroke (NINDS). The data used for the analyses described in this manuscript were in part obtained from the GTEx Portal V7 data repository. The results shown here are in part based on data generated by The Cancer Genome Atlas Research Network (https://www.cancer.gov/tcga) accessed via the R 'recount' package on Bioconductor. Protein expression in human tissues was queried using the Human Protein Atlas repository available online (http://www.proteinatlas.org). The content is solely the responsibility of the authors and does not necessarily represent the official views of the National Institutes of Health.

Contributors Conception and design: ZAL-B and CGD. Design of methodology: ZAL-B. Acquisition of data (provided animals, acquired and managed patients and provided facilities): ZAL-B, AO, TRN, LC, RM, HBL, ESA, and MCH. Analysis and interpretation of data (eg, statistical analysis, biostatistics and computational analysis): ZAL-B, AO, LC, TOD, UL, MMS, and MCH. Writing and/or revision of the manuscript: ZAL-B and CGD. Administrative, technical, or material support (ie, reporting or organizing data, constructing databases): AP, TRN, RM, JCZ, RR, MKS, PM, MMS, and MCH. Study supervision: CGD. All authors reviewed and approved the manuscript.

Funding This study was supported by the US National Institutes of Health National Cancer Institute (CA127153 to CD, CA238005 to MMS, and CA237623 to JCZ); the US Department of Defense (W81XWH-13-1-0369); the Patrick C. Walsh Fund; the OneInSix Foundation; the Swiss National Science Foundation (Early Postdoc Mobility Fellowship to AP: P2ZHP3 181557); the National Science Foundation (fellowship to LC: DGE 16-44869); the Prostate Cancer Foundation (PCF Challenge Awards to CGD and MMS, and Young Investigator Awards to HBL and JCZ) and the National Institute of Health Cancer Center Support Grants P30 CA013696 and P30 CA006973).

Competing interests CD has served as a consultant for Agenus, BMS, Dendreon, Janssen Oncology, Eli Lilly, F-Star, Merck, AstraZeneca, MedImmune, Pierre Fabre, Genentech, and Genocea Biosciences, and has stock or ownership interests in Compugen, Harpoon, Kleo, and Tizona Therapeutics. PM has served as a consultant for AstraZeneca, Medimmune and ATARA Biotherapeutics Inc. EA has served as a paid consultant/advisor to Janssen, Pfizer, Sanofi, Dendreon, Bayer, Bristol Myers Squibb, Amgen, Merck, AstraZeneca, and Clovis; has received research grants to his institution from Janssen, Johnson &Johnson, Sanofi, Bristol Myers Squibb, Pfizer, AstraZeneca, Celgene, Merck, Bayer, Clovis; and is an inventor of a biomarker technology that has been licensed to Qiagen. RR has served as a consultant to Gilead, Atara, Novartis, Celgene, Monsanto and Magenta. UL has served as a founder to and owns stock in Alchemab Therapeutics and Patch Biosciences.

Patient consent for publication Not required.

Ethics approval The Institutional Review Board of the Johns Hopkins Sidney Kimmel Comprehensive Cancer Center (Baltimore, Maryland) provided ethical approval for the use of patient materials in this study (IRB # NA_00073453).

Provenance and peer review Not commissioned; externally peer reviewed.

Data availability statement Data are available in a public, open access repository. The datasets analyzed during the current study are available in the NCBI Gene Expression Omnibus repository, the Genotype-Tissue Expression Portal V7 data repository, the Functional Annotation of the Mammalian Genome data repository, the Human Protein Atlas repository, and the cBioPortal for cancer genomics.

Supplemental material This content has been supplied by the author(s). It has not been vetted by BMJ Publishing Group Limited (BMJ) and may not have been peer-reviewed. Any opinions or recommendations discussed are solely those of the author(s) and are not endorsed by BMJ. BMJ disclaims all liability and responsibility arising from any reliance placed on the content. Where the content includes any translated material, BMJ does not warrant the accuracy and reliability of the translations (including but not limited to local regulations, clinical guidelines, terminology, drug names and drug dosages), and is not responsible for any error and/or omissions arising from translation and adaptation or otherwise.

Open access This is an open access article distributed in accordance with the Creative Commons Attribution Non Commercial (CC BY-NC 4.0) license, which permits others to distribute, remix, adapt, build upon this work non-commercially, and license their derivative works on different terms, provided the original work is properly cited, appropriate credit is given, any changes made indicated, and the use is non-commercial. See http://creativecommons.org/licenses/by-nc/4.0/.

ORCID iDs
Zoila A Lopez-Bujanda http://orcid.org/0000-0001-5729-7309
Aleksandar Obradovic http://orcid.org/0000-0002-8009-0186
Thomas R Nirschl http://orcid.org/0000-0002-3329-6229

Rodney Macedo http://orcid.org/0000-0001-6252-7703
Alexandros Papachristodoulou http://orcid.org/0000-0001-8488-7785
Uri Laserson http://orcid.org/0000-0002-8429-7686
Ran Reshef http://orcid.org/0000-0003-2185-9546
Emmanuel S Antonarakis http://orcid.org/0000-0003-0031-9655
Michael C Haffner http://orcid.org/0000-0003-0809-6425
Michael M Shen http://orcid.org/0000-0002-4042-1657
Pawel Muranski http://orcid.org/0000-0002-4446-6385
Charles G Drake http://orcid.org/0000-0001-9610-3677

REFERENCES

1 Ji G, Huang C, Song G, *et al*. Are the pathological characteristics of prostate cancer more aggressive or more indolent depending upon the patient age? *Biomed Res Int* 2017;2017:1438027. 2017.
2 Scher HI, Morris MJ, Stadler WM, *et al*. Trial design and objectives for castration-resistant prostate cancer: updated recommendations from the prostate cancer clinical trials Working group 3. *J Clin Oncol* 2016;34:1402–18.
3 Comiskey MC, Dallos MC, Drake CG. Immunotherapy in prostate cancer: teaching an old dog new tricks. *Curr Oncol Rep* 2018;20:75.
4 Venturini NJ, Drake CG. Immunotherapy for prostate cancer. *Cold Spring Harb Perspect Med* 2019;9. doi:10.1101/cshperspect.a030627. [Epub ahead of print: 01 May 2019].
5 Small EJ, Schellhammer PF, Higano CS, *et al*. Placebo-Controlled phase III trial of immunologic therapy with sipuleucel-T (APC8015) in patients with metastatic, asymptomatic hormone refractory prostate cancer. *J Clin Oncol* 2006;24:3089–94.
6 Higano CS, Schellhammer PF, Small EJ, *et al*. Integrated data from 2 randomized, double-blind, placebo-controlled, phase 3 trials of active cellular immunotherapy with sipuleucel-T in advanced prostate cancer. *Cancer* 2009;115:3670–9.
7 Kantoff PW, Higano CS, Shore ND, *et al*. Sipuleucel-T immunotherapy for castration-resistant prostate cancer. *N Engl J Med* 2010;363:411–22.
8 Lee P, Gujar S. Potentiating prostate cancer immunotherapy with oncolytic viruses. *Nat Rev Urol* 2018;15:235–50.
9 de Almeida DVP, Fong L, Rettig MB, *et al*. Immune checkpoint blockade for prostate cancer: niche role or next breakthrough? *Am Soc Clin Oncol Educ Book* 2020;40:1–18.
10 Kiessling A, Wehner R, Füssel S, *et al*. Tumor-Associated antigens for specific immunotherapy of prostate cancer. *Cancers* 2012;4:193–217.
11 Obradovic AZ, Dallos MC, Zahurak ML, *et al*. T-Cell infiltration and adaptive Treg resistance in response to androgen deprivation with or without vaccination in localized prostate cancer. *Clin Cancer Res* 2020;26:3182–92.
12 Antonarakis ES, Zahurak M, Schaeffer EM, *et al*. Neoadjuvant randomized trial of degarelix (Deg) ± cyclophosphamide/GVAX (Cy/GVAX) in men with high-risk prostate cancer (PCA) undergoing radical prostatectomy (Rp). *JCO* 2017;35:5077 doi:10.1200/JCO.2017.35.15_suppl.5077
13 TGM4. Available: https://www.proteinatlas.org/ENSG00000163810-TGM4/tissue
14 FOLH1/PSMA. Available: https://www.proteinatlas.org/ENSG00000086205-FOLH1/tissue
15 Pontén F, Jirström K, Uhlen M. The Human Protein Atlas--a tool for pathology. *J Pathol* 2008;216:387–93.
16 Uhlén M, Fagerberg L, Hallström BM, *et al*. Proteomics. tissue-based map of the human proteome. *Science* 2015;347:1260419.
17 Xu GJ, Shah AA, Li MZ, *et al*. Systematic autoantigen analysis identifies a distinct subtype of scleroderma with coincident cancer. *Proc Natl Acad Sci U S A* 2016;113:E7526–34.
18 Mohan D, Wansley DL, Sie BM, *et al*. PhIP-Seq characterization of serum antibodies using oligonucleotide-encoded peptidomes. *Nat Protoc* 2018;13:1958–78.
19 Lopez-Bujanda ZA, Haffner MC, Chaimowitz MG, *et al*. Castration-mediated IL-8 promotes myeloid infiltration and prostate cancer progression. *Nat Cancer* 2021;in press. doi:10.1038/s43018-021-00227-3
20 Rao V, Heard JC, Ghaffari H, *et al*. A Hoxb13-driven reverse tetracycline transactivator system for conditional gene expression in the prostate. *Prostate* 2012;72:1045–51.
21 Ritchie ME, Phipson B, Wu D, *et al*. limma powers differential expression analyses for RNA-sequencing and microarray studies. *Nucleic Acids Res* 2015;43:e47.
22 Team. *R, C. R: a language and environment for statistical computing*. Vienna, Austria: R Foundation for Statistical Computing, 2014.
23 Wickham H. *ggplot2: elegant graphics for data analysis*. eBook, 2016.
24 Crowley L, Cambuli F, Aparicio L, *et al*. A single-cell atlas of the mouse and human prostate reveals heterogeneity and conservation of epithelial progenitors. *Elife* 2020;9. doi:10.7554/eLife.59465. [Epub ahead of print: 11 Sep 2020].
25 Lizio M, Abugessaisa I, Noguchi S, *et al*. Update of the FANTOM web resource: expansion to provide additional transcriptome atlases. *Nucleic Acids Res* 2019;47:D752–8.
26 . The Genotype-Tissue expression (GTEx) project. *Nat Genet* 2013;45:580–5.
27 Wang ZA, Mitrofanova A, Bergren SK, *et al*. Lineage analysis of basal epithelial cells reveals their unexpected plasticity and supports a cell-of-origin model for prostate cancer heterogeneity. *Nat Cell Biol* 2013;15:274–83.
28 Taylor BS, Schultz N, Hieronymus H, *et al*. Integrative genomic profiling of human prostate cancer. *Cancer Cell* 2010;18:11–22.
29 Kassambara A KM, Biecek P, Fabian S. *Package 'survminer'. Version 0.4.3 ed2018*, 2018.
30 Melville LMaJHaJ. UMAP: uniform manifold approximation and projection for dimension reduction. *arXiv* 2018.
31 Van Gassen S, Callebaut B, Van Helden MJ, *et al*. FlowSOM: using self-organizing maps for visualization and interpretation of cytometry data. *Cytometry A* 2015;87:636–45.
32 Langmead B, Salzberg SL. Fast gapped-read alignment with Bowtie 2. *Nat Methods* 2012;9:357–9.
33 Wang X, Kruithof-de Julio M, Economides KD, *et al*. A luminal epithelial stem cell that is a cell of origin for prostate cancer. *Nature* 2009;461:495–500.
34 Meeker AK, Hicks JL, Platz EA, *et al*. Telomere shortening is an early somatic DNA alteration in human prostate tumorigenesis. *Cancer Res* 2002;62:6405–9.
35 Koh CM, Bieberich CJ, Dang CV, *et al*. Myc and prostate cancer. *Genes Cancer* 2010;1:617–28.
36 Brooks JD, Weinstein M, Lin X, *et al*. Cg island methylation changes near the GSTP1 gene in prostatic intraepithelial neoplasia. *Cancer Epidemiol Biomarkers Prev* 1998;7:531–6.
37 Dubbink HJ, Verkaik NS, Faber PW, *et al*. Tissue specific and androgen-regulated expression of human prostate-specific transglutaminase. *Biochem J* 1996;315 (Pt 3:901–8.
38 Evans MJ, Smith-Jones PM, Wongvipat J, *et al*. Noninvasive measurement of androgen receptor signaling with a positron-emitting radiopharmaceutical that targets prostate-specific membrane antigen. *Proc Natl Acad Sci U S A* 2011;108:9578–82.
39 Calcinotto A, Spataro C, Zagato E, *et al*. Il-23 secreted by myeloid cells drives castration-resistant prostate cancer. *Nature* 2018;559:363–9.
40 van der Toom EE, Axelrod HD, de la Rosette JJ, *et al*. Prostate-Specific markers to identify rare prostate cancer cells in liquid biopsies. *Nat Rev Urol* 2019;16:7–22.
41 Dahlman A, Edsjö A, Halldén C, *et al*. Effect of androgen deprivation therapy on the expression of prostate cancer biomarkers MSMB and MSMB-binding protein CRISP3. *Prostate Cancer Prostatic Dis* 2010;13:369–75.
42 Tiwari R, Manzar N, Bhatia V, *et al*. Androgen deprivation upregulates SPINK1 expression and potentiates cellular plasticity in prostate cancer. *Nat Commun* 2020;11:384.
43 Cao Z, Wang Y, Liu Z-Y, *et al*. Overexpression of transglutaminase 4 and prostate cancer progression: a potential predictor of less favourable outcomes. *Asian J Androl* 2013;15:742–6.
44 Larman HB, Laserson U, Querol L, *et al*. PhIP-Seq characterization of autoantibodies from patients with multiple sclerosis, type 1 diabetes and rheumatoid arthritis. *J Autoimmun* 2013;43:1–9.
45 Larman HB, Zhao Z, Laserson U, *et al*. Autoantigen discovery with a synthetic human peptidome. *Nat Biotechnol* 2011;29:535–41.
46 GuhaThakurta D, Sheikh NA, Fan L-Q, *et al*. Humoral immune response against nontargeted tumor antigens after treatment with Sipuleucel-T and its association with improved clinical outcome. *Clin Cancer Res* 2015;21:3619–30.
47 Antonarakis ES, Kibel AS, Yu EY, *et al*. Sequencing of Sipuleucel-T and androgen deprivation therapy in men with hormone-sensitive biochemically recurrent prostate cancer: a phase II randomized trial. *Clin Cancer Res* 2017;23:2451–9.
48 Antonarakis ES, Small EJ, Petrylak DP, *et al*. Antigen-Specific CD8 lytic phenotype induced by Sipuleucel-T in hormone-sensitive or castration-resistant prostate cancer and association with overall survival. *Clin Cancer Res* 2018;24:4662–71.
49 Wargowski E, Johnson LE, Eickhoff JC, *et al*. Prime-Boost vaccination targeting prostatic acid phosphatase (PAP) in patients with metastatic castration-resistant prostate cancer (mCRPC) using Sipuleucel-T and a DNA vaccine. *J Immunother Cancer* 2018;6:21.

50 Hagihara K, Chan S, Zhang L, *et al*. Neoadjuvant sipuleucel-T induces both Th1 activation and immune regulation in localized prostate cancer. *Oncoimmunology* 2019;8:e1486953.
51 Kloss CC, Lee J, Zhang A, *et al*. Dominant-Negative TGF-β receptor enhances PSMA-Targeted human CAR T cell proliferation and augments prostate cancer eradication. *Mol Ther* 2018;26:1855–66.
52 Junghans RP, Ma Q, Rathore R, *et al*. Phase I trial of Anti-PSMA designer CAR-T cells in prostate cancer: possible role for interacting interleukin 2-T cell pharmacodynamics as a determinant of clinical response. *Prostate* 2016;76:1257–70.
53 Morgenroth A, Cartellieri M, Schmitz M, *et al*. Targeting of tumor cells expressing the prostate stem cell antigen (PSCA) using genetically engineered T-cells. *Prostate* 2007;67:1121–31.
54 Mahadevan M, Liu Y, You C, *et al*. Generation of robust cytotoxic T lymphocytes against prostate specific antigen by transduction of dendritic cells using protein and recombinant adeno-associated virus. *Cancer Immunol Immunother* 2007;56:1615–24.
55 Zhang D, Zhao S, Li X, *et al*. Prostate luminal progenitor cells in development and cancer. *Trends Cancer* 2018;4:769–83.
56 Rivera-Gonzalez GC, Droop AP, Rippon HJ, *et al*. Retinoic acid and androgen receptors combine to achieve tissue specific control of human prostatic transglutaminase expression: a novel regulatory network with broader significance. *Nucleic Acids Res* 2012;40:4825–40.
57 Shaikhibrahim Z, Lindstrot A, Buettner R, *et al*. Analysis of laser-microdissected prostate cancer tissues reveals potential tumor markers. *Int J Mol Med* 2011;28:605–11.
58 An G, Meka CS, Bright SP, *et al*. Human prostate-specific transglutaminase gene: promoter cloning, tissue-specific expression, and down-regulation in metastatic prostate cancer. *Urology* 1999;54:1105–11.
59 Sequeiros T, Rigau M, Chiva C, *et al*. Targeted proteomics in urinary extracellular vesicles identifies biomarkers for diagnosis and prognosis of prostate cancer. *Oncotarget* 2017;8:4960–76.
60 Cho S-Y, Choi K, Jeon J-H, *et al*. Differential alternative splicing of human transglutaminase 4 in benign prostate hyperplasia and prostate cancer. *Exp Mol Med* 2010;42:310–8.
61 Jiang WG, Ye L, Sanders AJ, *et al*. Prostate transglutaminase (TGase-4, TGaseP) enhances the adhesion of prostate cancer cells to extracellular matrix, the potential role of TGase-core domain. *J Transl Med* 2013;11:269.
62 Ablin RJ, Owen S, Jiang WG. Prostate transglutaminase (TGase-4) induces epithelial-to-mesenchymal transition in prostate cancer cells. *Anticancer Res* 2017;37:481–7.
63 Landegren N, Sharon D, Shum AK, *et al*. Transglutaminase 4 as a prostate autoantigen in male subfertility. *Sci Transl Med* 2015;7:ra101.
64 Dieterich W, Ehnis T, Bauer M, *et al*. Identification of tissue transglutaminase as the autoantigen of celiac disease. *Nat Med* 1997;3:797–801.
65 Sárdy M, Kárpáti S, Merkl B, *et al*. Epidermal transglutaminase (TGASE 3) is the autoantigen of dermatitis herpetiformis. *J Exp Med* 2002;195:747–57.
66 Hadjivassiliou M, Aeschlimann P, Strigun A, *et al*. Autoantibodies in gluten ataxia recognize a novel neuronal transglutaminase. *Ann Neurol* 2008;64:332–43.
67 Lopez-Bujanda Z, Drake CG. Myeloid-Derived cells in prostate cancer progression: phenotype and prospective therapies. *J Leukoc Biol* 2017;102:393–406.
68 Bilusic M, Madan RA, Gulley JL. Immunotherapy of prostate cancer: facts and hopes. *Clin Cancer Res* 2017;23:6764–70.
69 Zahm CD, Colluru VT, McNeel DG. Dna vaccines for prostate cancer. *Pharmacol Ther* 2017;174:27–42.
70 Patel A, Fong L. Immunotherapy for Prostate Cancer: Where Do We Go From Here?-PART 1: Prostate Cancer Vaccines. *Oncology* 2018;32:112–20.
71 Collins JM, Redman JM, Gulley JL. Combining vaccines and immune checkpoint inhibitors to prime, expand, and facilitate effective tumor immunotherapy. *Expert Rev Vaccines* 2018;17:697–705.
72 Lopez-Bujanda ZA, Chaimowitz MG, Armstrong TD, *et al*. Robust antigen-specific CD8 T cell tolerance to a model prostate cancer neoantigen. *Oncoimmunology* 2020;9:1809926.
73 Cancer Genome Atlas Research Network. The molecular taxonomy of primary prostate cancer. *Cell* 2015;163:1011–25. doi:10.1016/j.cell.2015.10.025